Food Research International 188 (2024) 114475

Contents lists available at ScienceDirect

Food Research International

journal homepage: www.elsevier.com/locate/foodres

Chitosan-based nanocomposite films with carnauba wax, rosin resin, and zinc oxide nanoparticles

Luiz Carlos Corrêa-Filho [a,*], Jailton Ribeiro dos Santos Junior [a], Andresa Viana Ramos [b], Ana Paula Martinazzo [c], Alberto Claudio Habert [b,d], Carlos Wanderlei Piler de Carvalho [e], Antônio Gomes Soares [e], Renata Valeriano Tonon [e], Lourdes Maria Corrêa Cabral [e]

[a] Graduate Program in Food Science and Technology, Federal Rural University of Rio de Janeiro, 23890-000 Seropédica, RJ, Brazil
[b] Nanotechnology Engineering Program, COPPE, Federal University of Rio de Janeiro, 21941-972 Rio de Janeiro, RJ, Brazil
[c] Department of Agribusiness Engineering, Federal Fluminense University, 27255-125 Volta Redonda, RJ, Brazil
[d] Chemical Engineering Program, COPPE, Federal University of Rio de Janeiro, 21941-972 Rio de Janeiro, RJ, Brazil
[e] Embrapa Food Technology, Guaratiba, 23020- 470 Rio de Janeiro, RJ, Brazil

ARTICLE INFO

Keywords:
Biodegradable films
Polymers
Active packaging
Barrier properties
Mechanical properties

ABSTRACT

This work aimed to develop edible emulsion-based barriers in the form of chitosan composite films, with a focus on assessing the impacts of carnauba wax, rosin resin, and zinc oxide nanoparticles on their properties. Six films were produced by casting using chitosan as polymer base and glycerol as plasticizer. Acetic acid and polysorbate 80 were also used to facilitate the dissolution and mixing of the components. The six filmogenic solutions contained chitosan at 1.2% w/v, wax or resin content with 0 or 0.6% m/v and ZnO with 0 or 0.05% m/v. The dried films were characterized according to their chemical, barrier, mechanical, thermal and optical properties. All treatments resulted in flexible films. Chitosan films appeared smoother and more uniform under SEM imaging, while carnauba wax films displayed roughness due to their hydrophobic nature. Wax and resin films were less transparent and water soluble than the chitosan-only films. On the other hand, the addition of ZnO in the formulations increased the solubility of the films. The sorption degree was in line with the solubility results, i.e., films with ZnO presented higher sorption degree and solubility values. All treatments showed low or non-light UV transmission, indicating that the films provide good barrier to UV light. In the visible light region, films of resin with ZnO showed the lowest transmittance values, hence offering a good barrier to visible light. Among the evaluated films, chitosan, and resin films with ZnO nanoparticles were more rigid and resistant to deformation. Overall, films produced with rosin resin and ZnO nanoparticles showed potential improvements in barrier, mechanical, thermal, and optical properties, mainly due to their low water solubility, good UV protection and low permeability to water vapor and oxygen, which are suitable for using in formulations, intended to produce edible films and coatings.

1. Introduction

In response to growing consumer demand for safe, high-quality products and a preference for manufacturers with robust risk control practices, researchers have focused on substituting synthetic additives with more natural alternatives that are less detrimental to both consumer health and the environment. (Asioli et al., 2017; Mesías et al., 2021).

The development of active biopolymeric films aligns with these aspirations, effectively addressing two significant concerns. First, it reduces reliance on conventional plastic packaging. Second, it accomplishes this by incorporating agents known for their antimicrobial and antioxidant properties, such as essential oils or metallic oxides. This innovative approach not only enhances product safety but also promotes sustainability in packaging, meeting the dual objectives of quality and environmental responsibility.(Kamarudin et al., 2022; Khalid & Arif, 2022; Moeini et al., 2021).

Biopolymer materials have emerged as a sustainable alternative to replace petroleum-based packaging materials. They are highly sought after due to their abundance, renewability, eco-friendliness,

* Corresponding author.
E-mail address: luizcorrea@id.uff.br (L.C. Corrêa-Filho).

https://doi.org/10.1016/j.foodres.2024.114475
Received 17 November 2023; Received in revised form 19 March 2024; Accepted 7 May 2024
Available online 10 May 2024

biodegradability, and biocompatibility, effectively addressing the pressing environmental and food safety concerns associated with conventional packaging materials. In packaging formulations, various biopolymers have found applications, including pectin, starch, gums, waxes, and chitosan, demonstrating the versatility and potential of these materials in meeting the demands of a more sustainable and responsible packaging industry (Lin et al., 2023; Shankar & Rhim, 2016).

Chitosan, a widely used edible biopolymer derived from the deacetylation of chitin, has been studied for its ability to produce high-performance films and coatings due to its effectiveness against bacterial, fungal, and viral pathogen (Díaz-montes and Castro-muñoz, 2021; Priyadarshi & Rhim, 2020; Terzioğlu et al., 2021; Hongxia Wang et al., 2021). The use of composite films of chitosan with hydrophobic compounds, such as lipids, offers an alternative method to enhance water barrier properties (Santacruz et al., 2015). In pursuit of enhanced water barrier properties, various composites have been created by blending polysaccharides with lipids. Among these lipids, carnauba wax, derived from the Brazilian palm tree, has gained significant prominence as an edible coating to extend the shelf life of fruits and vegetables. Its high melting point and hardness make it ideal for developing durable coatings. Additionally, carnauba wax is primarily employed to reduce water loss while providing a glossy appearance (Butt et al., 2023; Susmita Devi et al., 2022).

Another hydrophobic component employed to enhance water vapor resistance is rosin resin, extracted from pine exudates and primarily composed of abietic acid. With an amorphous structure, though some reports suggest some crystallinity, its melting point typically falls between 70 to 78 °C. Rosin resin is frequently utilized as a modifier or coating to enhance water resistance and visual appeal, thanks to its strong hydrophobic properties and glossy finish. (Cruces et al., 2021; Su et al., 2021).

In general, biopolymeric films typically exhibit a hydrophilic nature and limited mechanical and thermal properties, which can hinder their effectiveness in various applications. As a result, it often becomes necessary to apply specific techniques to enhance these attributes. (Xavier et al., 2020). One promising approach involves leveraging nanotechnology, such as the incorporation of zinc oxide nanoparticles, in active packaging, directly contributing to the stability of packaged foods (de Coelho et al., 2020; Mohammadi et al., 2019). The utilization of ZnO nanoparticles can augment both the mechanical strength and barrier properties of polymeric films, in addition to providing antimicrobial benefits (Espitia and de Soares, 2012; Porto et al., 2018).

The study focuses on the development of chitosan-based edible barriers, incorporating carnauba wax, rosin resin and zinc oxide nanoparticles. To the best of our knowledge, there is no report on the comparison among the effect of these three additives on film properties, encompassing chemical, barrier, mechanical, thermal behaviour, and optical properties. Hence, the objective of this research was to craft chitosan films, with a focus on assessing the impacts of carnauba wax, rosin resin, and zinc oxide nanoparticles on their properties.

2. Material and methods

2.1. Materials

Medium molecular weight chitosan (MW = 190-310kDA, purity ≥ 75 %, deacetylation degree of 75–85 %, and a viscosity of 200–800 cPs), zinc oxide nanoparticles (nanopowder, <100 nm particle size, 97 % purity), and acetic acid (Glacial, 100 % Anhydrous, 99.8 % purity) were purchased from Sigma–Aldrich (St. Louis, EUA). Carnauba wax type 1 and rosin resin were purchased from Fenix Ceras e Produtos derivados LTDA (São Paulo, Brazil). Glycerol (99 % purity) was purchased from Vetec Química Fina LTDA (Rio de Janeiro, Brazil) and polysorbate 80 (purity ≥ 90 %) was purchased from Neon reagents analytic LTDA (São Paulo, Brazil).

2.2. Film formulation

The films were prepared by casting technique, following the methodology utilized by Dos Santos et al. (2017) with some modifications. To prepare chitosan film-forming solution, 1.2 % (w/v) of chitosan was dissolved in a 1 % (v/v) acetic acid solution with the assistance of an ultra-turrax (IKA-Werke GmbH & Co., Germany). This solution was then enriched with 25 % (w/w) polysorbate 80 and 30 % (w/w) glycerol.

Composite films were produced by adding rosin resin, carnauba wax, or ZnO to 200 mL of a 1 % (v/v) acetic acid solution, which was subsequently combined with the chitosan film-forming solution. 50 % wt. of rosin resin or carnauba wax were dissolved at 80 °C, while ZnO (0.5 % wt.) was dispersed using an ultrasound bath.

Pure Chitosan films(C), chitosan-zinc oxide nanocomposite films (CZn), chitosan-carnauba wax composite films (CW), chitosan-carnauba wax-ZnO nanocomposite films (CWZn), chitosan-rosin resin composite films (CR) and chitosan-rosin resin-ZnO nanocomposite films (CRZn) were prepared.

The film-forming solutions were poured into petri dishes and dried in a fan oven at 30 °C. Once the films were ready, they were preconditioned in desiccators at 53 % relative humidity, maintained by a saline solution saturated with magnesium nitrate ($Mg(NO_3)_2{\cdot}6H_2O$), to assure that all the films were stored in the same conditions of relative humidity before analysis, in order to allow for an adequate comparison among them (Shankar et al., 2018): film thickness and water solubility, optical and mechanical properties, X-ray diffraction, thermogravimetric analysis, Differential Scanning Calorimetry, and gas permeability.

2.3. Films characterization

2.3.1. Film thickness and water solubility

Film thickness was measured to the nearest 0.001 mm by using a digital micrometrer, IP 54 (Fowler, Newton, USA), at nine points: one at the centre and eight at opposite positions. All measurements were performed in triplicate.

Solubility and swelling in water were performed according to the methodology described by Mei et al. (2013). 20 x 20 mm film samples were cut and dried in a fan oven at 105 °C for 24 h to determine the initial dry mass (M_0). Afterwards, the dry film samples were immersed in 50 mL of distilled water and stirred at a constant rotation speed of 65 rpm at 30 °C in a shaker incubator SL-222/E (Solab, Piracicaba, Brazil). After 24 h, the wet weight of the film samples (M_1) was measured immediately by pulling the films out of the water and slightly removing the water on the surface with an absorbent paper. Finally, the samples were dried in a fan oven at 105 °C for 24 h and weighed to determine the final dry mass (M_2). Measurements were determined in triplicate.

The solubility and degree of swelling of the films were calculated according to equations (1) and (2), respectively.

$$\text{Swelling}\,(\%) = \frac{(M_1 - M_0)}{M_0} \times 100 \quad (1)$$

where M_0 is the initial film mass and M_1 represents the film mass after the swelling time.

$$\text{Solubility}\,(\%) = \frac{(M_0 - M_2)}{M_0} \times 100 \quad (2)$$

where M_0 represents the initial film mass and M_2 is the final dry mass.

2.3.2. Moisture content

Moisture content was measured by drying samples of 20 mm × 20 mm at 105 °C in a fan oven Model MA 035/3 (Marconi, São Paulo, Brazil) for 24 h and determined as a fraction of initial film weight lost. Measurements were carried out in triplicate.

2.3.3. Optical properties

Ultraviolet (UV) and visible light barrier properties were measured on films at selected wavelengths in a range between 200–800 nm using a UV spectrophotometer UV M−51 (BEL, Monza, Italy). The film was cut into 10 mm × 40 mm size samples and attached to one side of colorimetric cup. Measures were made in triplicate and an empty colorimetric cup was used as reference. Opacity of films was calculated as a relationship between film absorbance in 600 nm and film thickness in mm.

2.3.4. Morphological characterization of films

The film surface and cross-section morphological structure was observed with a Quattro ESEM microscope (Thermo Fisher, Waltham, MA, USA) operated at 10 kV. The film samples were fixed on aluminium stubs with a carbon conductive adhesive tape and coated with a thin platinum layer.

2.3.5. Mechanical properties

Mechanical tests were performed using a texture analyser TA XT Plus (Stable Microsystems, Surrey, UK) with a load cell of 30 kg. For the tensile tests, the film samples with 100 mm x 20 mm were fixed in the equipment's grips with an initial distance of 50 mm, the tensile speed was 6 mm·min^{-1}. The tensile strength (TS), the elongation at break (EB) and Young's modulus (YM) were evaluated with a minimum of 10 replicates for each film and determined according to equations (4), 5 and 6, respectively. Tensile strength indicates the maximum tensile stress that the film can withstand, Young's modulus is a measure of film stiffness, and elongation at break is the maximum change in length of a specimen before breaking (Vieira et al., 2021).

$$TS = \frac{F_{max}}{L \times W} \tag{4}$$

F_{max} is the maximum tension during the stretching process. L is the width of the films, and W is the thickness.

$$EB = \frac{L_1 - L_0}{L_0} \times 100 \tag{5}$$

L_0 is the initial film length and L_1 is the film break length.

$$YM = \frac{\sigma}{\gamma} \tag{6}$$

σ is slope of the tensile curve and γ is deformation.

Puncture tests were analysed by measuring the puncture force (PF) and puncture deformation (PD) using a TA.TX plus Stable Micro Systems texture analyser (Surrey, England). A cylindrical probe of 5 mm diameter was moved perpendicular to the surface of the film samples with 25 mm x 25 mm at constant speed of 1 mm·s^{-1} until the probe passed through the film. The diameter of the area where film was placed was 10 mm. The PF and PD were determined through the force–deformation curves of at least ten specimens of each film sample. Puncture force was calculated as the maximum puncture force until the breaking point, and puncture deformation was reported as the maximum distance of deformation at the breaking point (Cazón et al., 2019).

2.3.6. Fourier transform infrared spectroscopy (FT-IR)

The FTIR spectra of the films samples were acquired, using a Agilent Cary 670 FTIR spectrometer (Agilent, Santa Barbara, CA, USA). The spectra (32 scans per spectrum) of samples were collected in duplicate in the mid-infrared wavenumber range from 4000 to 650 cm^{-1}, with a spectral resolution of 4 cm^{-1}.

2.3.7. X-ray diffraction (XRD)

The X-ray diffraction pattern of the films was obtained using a Bruker AXS D2 Phaser X-ray diffractometer (Bruker, Germany) with a CuKα radiation (λ = 1.5418 Å), at 30 kV and 10 mA. Films were scanned over the range of diffraction angle 2θ = 5 – 60°, with a scan speed of 2°/min at room temperature (Wu et al., 2019).

2.3.8. Thermogravimetric analysis (TGA)

Thermal behaviour of the films was determined using thermogravimetric analysis using a TGA-200 (Nova Instruments, South Carolina, USA), as described by Piñeros-Hernandez et al. (2017). Film samples with 500 mg were placed in porcelain crucibles and heated at a temperature range of 20 – 800 °C, at a rate of 10 °C·min^{-1}, under a nitrogen atmosphere with a flow rate of 50 mL·min^{-1}. Weight loss as a function of temperature (TG) and differential TG curves (DTG) were analysed. The experiments were carried out in triplicate.

2.3.9. Differential scanning calorimetry (DSC)

DSC analysis was performed to determine the amount of energy absorbed or released at different temperatures. The DSC curves of the films were accomplished in a Q200 DSC Differential Scanning Calorimetric module (TA Instruments, New Castle, USA), as described by Ghiasi et al. (2020). Film samples with 2 mg of known moisture content were placed in hermetically sealed aluminium pans and analysed at a heating rate of 10 °C·min^{-1} from −90 to 250 °C, in an internal atmosphere of nitrogen with a flow rate of 50 mL·min^{-1}.

2.3.10. Gas permeability

The CO_2 and O_2 gas permeability tests of the films followed the methodology proposed by García Jiménez et al. (2021). Pure gas permeation experiments consisted of applying a pressure differential to a film and then measuring the rate of pure gas flowing through it by increasing pressure in the permeate chamber.

The film sample was sealed in a 16.53 cm^3 cylindrical stainless steel permeation cell with a permeation area of 6.05 cm^2. Before starting the test, the pressure was increased in the feed side to achieve a pressure difference of 2 bar across the film. During the test, pressure variation data in the permeate side were recorded using LogChart II software until steady state was reached. The gas permeance was calculated with equation (7).

$$P = \left(\frac{T_{STP}}{T \times p_{STP}}\right) \bullet \left(\frac{V_s}{A \times l \times \Delta p}\right) \bullet \left(\frac{dp}{dt}\right) \tag{7}$$

Where P is the gas permeability in barrer $\left(1\ \text{barrer} = \frac{1\times10^{-10}\text{cm}^3[\text{STP}]\bullet\text{cm}}{\text{cm}^2\bullet\text{s}\bullet\text{cmHg}}\right)$, T_{STP}, and p_{STP} are the temperature and pressure at standard conditions, T is the permeation temperature (K), V_s is the volume of the permeate chamber (cm^3), A is the effective area of the membrane in the cell (cm^2), l is the film thickness (cm), Δp is the pressure difference between the feed and permeate sides (cmHg), $\left(\frac{dP}{dt}\right)$ is the steady state pressure rate in the permeate chamber (cmHg/s).

The water vapor permeability (WVP) of films was determined gravimetrically by using the modified ASTM E96-92 method (ASTM, 1993) as described by Rocha et al. (2014). Film samples were cut into circular shapes of 40 mm in diameter and sealed in permeation cells containing distilled water (100 % RH; 3,167 kPa water vapor pressure at 25 °C). The permeation cells were placed in desiccators containing blue silica gel (0 % RH; 0 Pa water vapor pressure at 25 °C) to ensure a water gradient in the system. Cells were weighed at 24 h intervals for 5 days. The water transferred through the film and adsorbed by the desiccant was determined from the weight loss of the permeation cell. The water vapor transmission rate was defined by the slope of the linear regression of weight loss versus time (g/h). The WVP was determined by the equation (8).

$$WVP = \frac{w}{t \bullet A} \times \frac{x}{\Delta p} \tag{8}$$

where WVP is water vapor permeability (g·mm·h^{-1}·m^{-2}·kPa^{-1}), w is the weight of permeation system (g), t is the time (h), x is the film thickness (mm), A is the area of exposed film, Δp is the difference of water vapor pressure through the film (kPa) at 25 °C. For each type of film, four

measurements of WVP were performed.

2.4. Statistical analysis

The data were subjected to analysis of variant (ANOVA) using the Statistica computer program Statistica version 10.0 (StatSoft Inc., Tulsa, USA). Post hoc multiple comparison was determined by the Tukey's test with the level of significance set at $p < 0.05$.

3. Results and discussion

3.1. Film thickness, moisture content, swelling and solubility in water

The film thickness ranged from 85.71 ± 5.35 to 152.86 ± 7.56 μm, with the greatest thickness observed in the carnauba wax films. As shown in Table 1, the addition of wax or resin to film formulations significantly increased film thickness. Akhtar et al. (2022) and Hromiš et al. (2015) also observed this increase in film thickness after the addition of lipid compounds in film-forming solutions. Dos Santos et al. (2017) reported that increasing the wax content also increases molecular contact between the matrix polymer and the wax compounds, which can weaken the aggregation forces of the polymeric chain, making the matrix more open.

The addition of wax, resin and ZnO decreased the moisture content of the films ($p < 0.05$), with the highest moisture content found in chitosan films (Table 1). Hromiš et al. (2015) also observed a decrease in moisture content after adding beeswax to chitosan-based films.

Conversely, CW and CR composite films exhibited no statistically significant differences in terms of thickness and moisture content when compared to their respective nanocomposite counterparts, CWZn and CRZn films. This suggests that the addition of ZnO did not lead to significant alterations in these particular properties. Furthermore, the addition of ZnO did not result in statistically significant changes in film thickness, and the reduction in moisture content in CZn films was less pronounced than in CR and CW films.

Solubility in water and swelling degree are indicators of the resistance of water (Yadav et al., 2021). Table 1 shows the water solubility of the films that ranged from 12.36 ± 0.08 % to 24.03 ± 0.50 %, with the lowest solubility found in wax films. All films were partially soluble maintaining their integrity during water immersion.

It was observed that the addition of ZnO nanoparticles, wax, or resin significantly decreased water solubility. Similar results were found for Soazo et al. (2013) and Dos Santos et al. (2017) after the incorporation of beeswax and carnauba wax in the film formulations, respectively. However, the greater effect on solubility in water can be attributed to the presence of carnauba wax. This can be associated to the predominant composition of carnauba wax, which primarily comprises a complex mixture of fatty esters and hydroxyacids. These constituents confer a high level of hydrophobicity and low wettability to the wax, thereby leading to the development of wax-polymer composites characterized by markedly reduced solubility in water (Reza et al., 2003; da Rocha et al., 2020).

The degree of swelling, on the other hand, was highly influenced by the presence of ZnO nanoparticles, as it can be seen on Table 1. The incorporation of ZnO nanoparticles might form a three-dimensional network of ZnO in the matrix polymer, which has been reported in literature for nanocomposite films (Al-Naamani et al., 2016; Hromiš et al., 2015; Yadav et al., 2021).

Table 1
Thickness, moisture content, water solubility, swelling and opacity of the films.

T	Thickness (μm)	Moisture content (%)	Solubility in Water (%)	Swelling (%)	Opacity (A600/mm)
C	$85.71^{c} \pm 5.35$	$32.21^{a} \pm 0.69$	$24.03^{a} \pm 0.50$	$76.53^{a} \pm 2.45$	$0.46^{d} \pm 0.07$
CZn	$92.86^{c} \pm 4.88$	$23.60^{b} \pm 0.55$	$18.45^{b} \pm 0.58$	$41.24^{d} \pm 2.27$	$0.77^{d} \pm 0.02$
CW	$148.57^{a} \pm 6.90$	$19.29^{d} \pm 0.03$	$13.61^{d} \pm 1.20$	$70.21^{b} \pm 0.15$	$2.09^{c} \pm 0.12$
CWZn	$152.86^{a} \pm 7.56$	$19.03^{d} \pm 0.32$	$12.36^{d} \pm 0.08$	$48.19^{c} \pm 1.77$	$2.31^{c} \pm 0.09$
CR	$115.71^{b} \pm 5.35$	$21.15^{c} \pm 0.02$	$18.13^{b} \pm 0.34$	$73.85^{a} \pm 3.20$	$3.09^{b} \pm 0.18$
CRZn	$122.86^{b} \pm 7.56$	$21.47^{c} \pm 0.60$	$16.47^{c} \pm 0.18$	$68.53^{b} \pm 0.94$	$3.51^{a} \pm 0.16$

*The means followed by the same letter, in the columns, do not differ from each other, according to Tukey's test at 5 % probability. T: Treatment; C: Chitosan; CZn: Chitosan + ZnO; CW: Wax; CWZn: Wax + ZnO; CR: Resin; CRZn: Resin + ZnO.

3.2. Optical properties – film opacity and UV/visible light barrier

The addition of wax or resin to the chitosan films and the addition of ZnO nanoparticles affected the light transmission profiles in the UV (250–350 nm) and visible (350–700 nm) ranges as depicted in Fig. 1.

Chitosan films showed the highest light transmittance, indicating that the chitosan film has a weak light barrier. However, the light barrier properties were favoured by the addition of ZnO, wax and resin.

All films showed excellent barrier to UV light, with a transmittance below 5 %. Additionally, it was observed that CR films exhibited a more substantial light barrier, resulting in a decrease in visible light transmittance of up to 40 %. In comparison, CW films displayed a reduced transmittance of up to 20 % when compared to pristine chitosan films. Similar results were reported by Zhang et al. (2018) in gelatine films with beeswax and carnauba wax. Exposure to visible and ultraviolet light causes oxidative deterioration of coated foods, leading to loss of nutrients and flavours. Therefore, optical properties are important characteristics for film applications, particularly if the film is used as a food coating or to improve product appearance (de Moraes Crizel et al., 2018; Martins et al., 2012).

Likewise, the light transmittance of films incorporated with ZnO nanoparticles are always lower than films without ZnO nanoparticles. These results are in line with Ngo et al., (2018) who evaluated the influence of the addition of different concentrations of zinc nanoparticles in pectin/alginate films. Yadav et al. (2021) also reported that the reinforcement of the chitosan film with ZnO particles loaded with gallic acid resulted in a polymer with better resistance to ultraviolet visible light than the polymer-only film, particularly when the nanoparticles are homogeneously dispersed in the polymeric matrix.

Film opacity values were between 0.50 and 3.41 mm^{-1}, with pure chitosan films exhibiting the lowest opacity value, as seen in Table 1. The addition of wax or resin to chitosan films significantly increased the

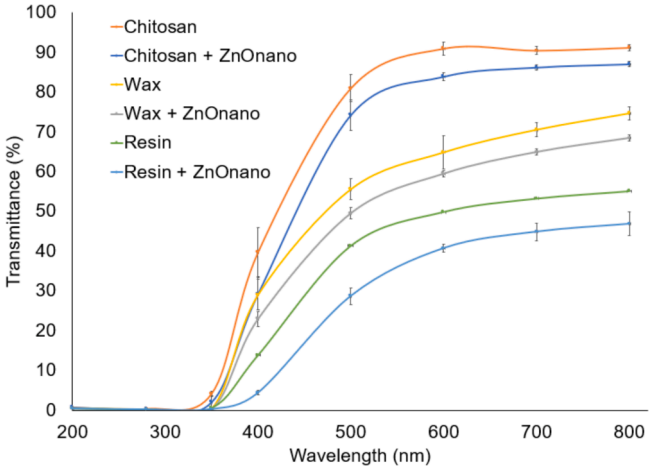

Fig. 1. Light transmission (%) at 200–800 nm of films.

opacity of the films. Dos Santos et al. (2017) reported that solid lipid particles, such as wax, introduce morphological heterogeneity in film emulsions. This heterogeneity, in turn, leads to the scattering of visible light within the films, contributing to their opacity. Fig. 2 shows the visual appearance of chitosan-based films.

The chitosan films were opaque, and the different treatments evaluated in this work resulted in films slightly different from the pure chitosan films. The greater visual changes were observed on CRZn, which were darker than the others. According to Sahraee et al. (2017), opaque films that limit UV and visible transmission are suitable polymers for packaging and food coatings, which can help reduce oxidation and light-induced discoloration.

3.3. Scanning electron microscopy (SEM)

The SEM images of the surface morphology and cross-section of the chitosan-based films are shown in Fig. 3. The surface and cross sections of the film samples exhibited different morphologies. Chitosan films showed smoother and more uniform surface than rosin or wax films. SEM images of chitosan films with rosin depicted the presence of rosin droplets dispersed within the chitosan matrix, suggesting the formation of an emulsion between chitosan and rosin, which rendered the mixture heterogeneous. Similar results were observed by Oliva-Moreno & Encinas (2021), who enhanced the water resistance of bioplastic pectin films by incorporating pine rosin. The authors observed the formation of rosin droplets dispersed in the pectin film. Films containing carnauba wax showed structural irregularities and roughness attributed to its hydrophobic characteristics. The rough surface of the film is linked to wax aggregation and lipid recrystallization occurring during the film drying process (Butt et al., 2023).

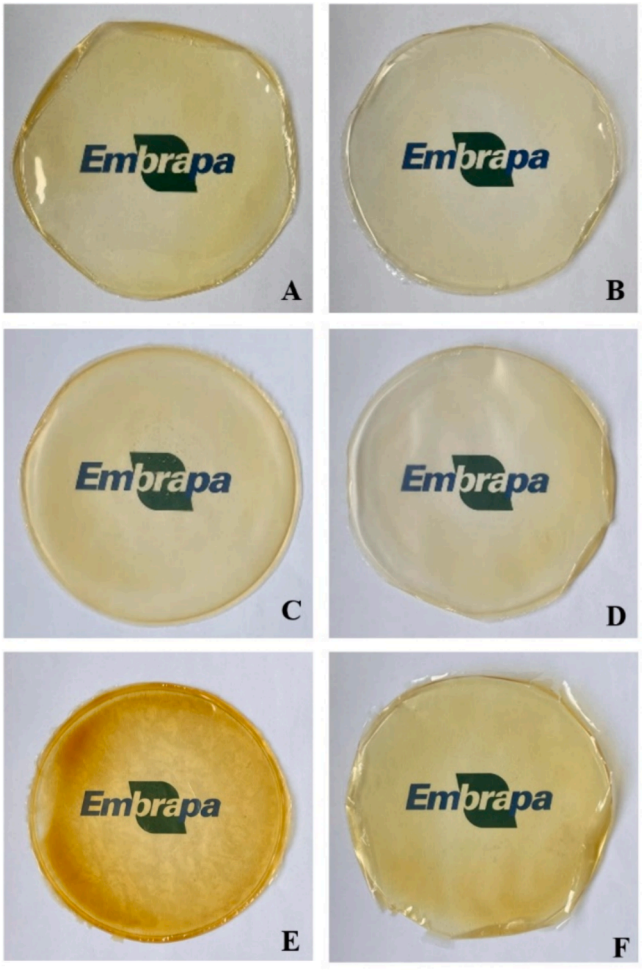

Fig. 2. Visual appearance of chitosan-based films. Chitosan + ZnO (A); Chitosan (B); Wax + ZnO (C); Wax (D); Resin + ZnO (E); Resin (F).

3.4. Mechanical properties

Mechanical properties are important to ensure adequate mechanical strength and integrity of the films during transport, handling and storage of food packaged with them (Vieira et al., 2021). The results presented in Table 2 showed that the addition of wax, resin and ZnO nanoparticles influenced the mechanical properties of the films.

The CZn films showed greater tensile strength, puncture force and Young's modulus, accompanied by a decrease in elongation at break. These results indicate that films with nanoparticles were more rigid and resistant to deformation. According to Wardana et al. (2018), the increase in tensile strength of nanocomposite films can be explained by the increase in the contact area between the matrix polymer and the ZnO nanoparticles. Also, the ability of the ZnO nanoparticles to fill the gap between the polymer chain, as well as limit the matrix movements, result in stiffer films (Meindrawan et al., 2018). Shankar et al., (2018) reported a 37.5 % increase in tensile strength of PLA composites and a slight decrease in elongation at break when 0.5 wt% ZnO nanoparticles were incorporated into PLA.

On the other hand, the mechanical properties of the resin films were not statistically different from the chitosan-only films except for the puncture deformation, which decreased due to the presence of resin. Interestingly, the resin had a more pronounced effect when combined with ZnO.

While CR films exhibited a puncture force like that of pure chitosan films and CZn films required a force approximately 80 % greater than chitosan films for puncture, CRZn films required only 18 % more force than pure chitosan films. This observation suggests a synergy between ZnO nanoparticles and rosin resin, impacting the film matrix and consequently influencing the mechanical resistance.

Carnauba wax promoted a decrease in tensile strength and Young's modulus, and increase in elongation at break, puncture force and puncture deformation at break. These results are in line with other reports of the effect of lipids in films (Cortés-Rodríguez et al., 2020; Pelissari et al., 2013).

Santos et al. (2014) also found the same behaviour in the mechanical properties of glycerol-plasticized emulsion films based on different combinations of cassava starch and carnauba wax. The authors attributed the decrease in tensile strength and Young's modulus to discontinuities in the polymeric matrix caused by the wax, implying a loss of cohesive forces, reducing the Youngs modulus. Butt et al. (2023), who produced films based on carnauba wax, incorporated sodium alginate in whey protein films and found low tensile resistant after increasing the lipid-based component.

The addition of carnauba wax decreased tensile strength and Young's modulus by 49 % and 60 %, respectively. This reduction may occur due to the fact that carnauba wax has a hydrophobic character, which may result in a porous matrix and the formation of wax agglomerates, as already observed by Gomes et al. (2019) in corn starch films with carnauba wax.

Young's modulus is an indicator of film rigidity, the higher the values the higher is film rigidity. While the addition of carnauba wax resulted in more flexibe films, the presence of ZnO nanoparticles resulted in films more rigid. According to Santos et al. (2014), lipid compounds may have plasticizing effects, favouring the elongation at break and impairing tensile strength. The reduced tensile strength and enhanced elongation at break have also been reported by Terzioğlu et al., (2021) for orange peel powder incorporated chitosan/polyvinyl alcohol composite films.

3.5. FT-IR

The structural configuration and functional groups of the chitosan-

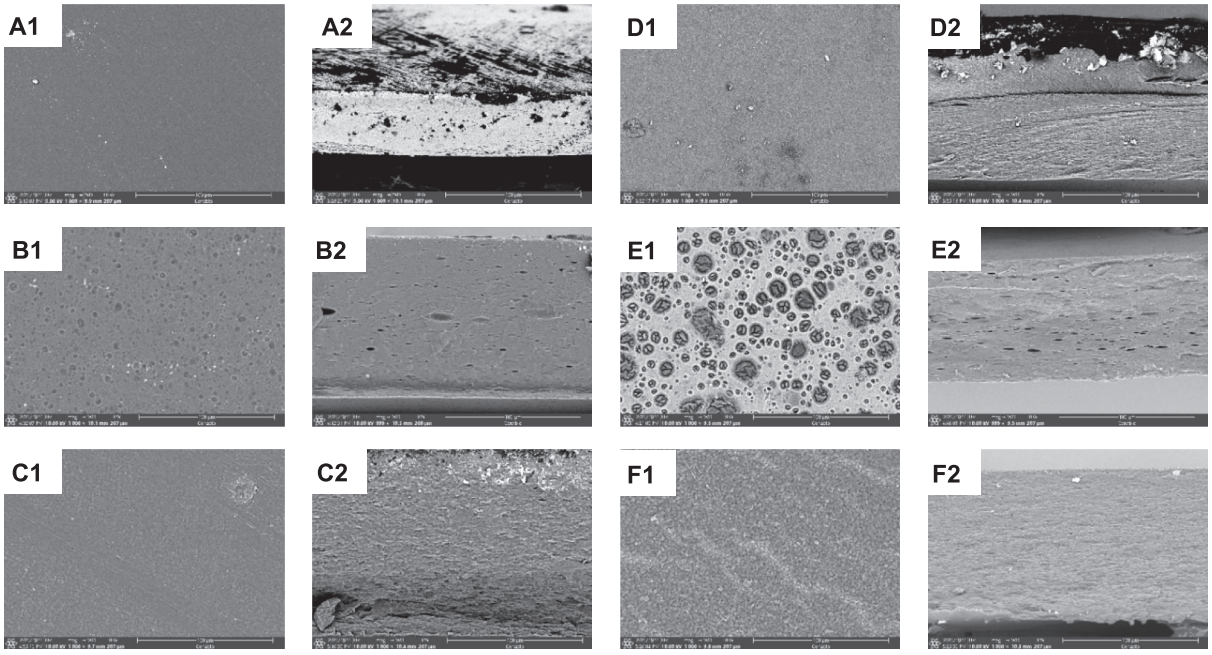

Fig. 3. SEM images of (A) Chitosan film, (B) Chitosan + Rosin film, (C) Chitosan + Wax film, (D) Chitosan + ZnO film, (E) Chitosan + Rosin + ZnO film and (F) Chitosan + Wax + ZnO film. (1) Surface image, (2) Cross-section image.

Table 2
Mechanical properties of the films.

T	Tensile strength (MPa)	Elongation at break (%)	Young's modulus (MPa)	Puncture force (N)	Puncture deformation (%)
C	21.99^{bc} ± 1.40	7.25^{bc} ± 0.92	13.48^{b} ± 1.99	31.89^{d} ± 2.67	5.52^{b} ± 0.29
CZn	36.74^{a} ± 3.03	3.39^{d} ± 1.00	21.12^{a} ± 2.05	57.59^{b} ± 4.04	4.73^{bc} ± 0.34
CW	11.46^{e} ± 1.18	14.25^{a} ± 1.97	5.45^{d} ± 0.40	42.66^{c} ± 6.79	9.61^{a} ± 1.02
CWZn	18.63^{d} ± 1.55	15.55^{a} ± 1.70	8.32^{c} ± 0.89	70.79^{a} ± 2.94	8.96^{a} ± 0.89
CR	19,86 ^{cd} ± 1.63	7.78^{b} ± 1.22	11.66^{b} ± 1.01	31.04^{d} ± 1.62	3.61 ^{cd} ± 0.44
CRZn	25.29^{b} ± 1.92	4.34 ^{cd} ± 0.71	20.74^{a} ± 1.38	37.69 ^{cd} ± 2.21	2.52^{d} ± 0.31

*The means followed by the same letter, in the columns, do not differ from each other, according to Tukey's test at 5 % probability. T: Treatment; C: Chitosan; CZn: Chitosan + ZnO; CW: Wax; CWZn: Wax + ZnO; CR: Resin; CRZn: Resin + ZnO.

based films were characterized by FT-IR spectroscopy. The main peaks of the chitosan-based films were similar, but some of the peaks were shifted and the intensity varied as shown in the FTIR spectra in Fig. 4.

The peak observed at 3239–3273 cm^{-1} (amide A) corresponds to the stretching vibrations of the NH single bond and the associated hydrogen bonding (Siripatrawan & Harte, 2010). The peaks at 2914–2922 cm^{-1} and 2847–2870 cm^{-1} represent the antisymmetric and symmetric stretching vibrations of CH_2 groups, respectively. The amide II band, occurring at 1541–1558 cm^{-1}, is attributed to NH bending and CN stretching vibrations, while the peak at 1381–1405 cm^{-1} corresponds to −C–N stretching within the amide group (Chen et al., 2016; L. Zhang et al., 2019). Furthermore, a peak in the range of 1021–1088 cm^{-1}, observed in all film samples, corresponds to the stretching vibration of the OH group in glycerol, which was used as a plasticizer (Y. Zhang et al., 2018).

The chitosan films with carnauba wax exhibited absorption bands associated with the functional groups present in the wax. Notably, sharp peaks were detected at 2914 and 2847 cm^{-1} in wax films. This observation aligns with findings by Y. Zhang et al. (2018), who reported similar characteristics in gelatin-based films upon the addition of carnauba wax. According to the authors, these peaks suggested the presence of fatty acid chains, attributed to the asymmetric and symmetric stretching vibrations of the aliphatic CN groups.

Furthermore, a new peak was observed in the spectrum of chitosan films with the addition of carnauba wax. This peak, observed at 1743 cm^{-1}, corresponds to the characteristic C = O stretching signals of fatty acid esters. Moreover, the addition of carnauba wax induced a shift in the peak absorption of O – H (stretching) and N – H (bending) signals in the chitosan film. Similar results were also found by Gutiérrez-Pacheco et al., (2020) in chitosan films with carnauba wax and oregano essential oil.

Regarding resin films, after the addition of rosin to the chitosan-resin films, a new band at 1699 cm^{-1} was observed, indicating the stretching vibrations of the C = O bond in rosin. Furthermore, the intensities of the –OH group stretching around 3280 cm^{-1} in the chitosan-resin films were weaker than those in films composed of chitosan-only. This suggests that the –OH groups of chitosan reacted with the carboxylic acid present in rosin. Additionally, the intensities of the peaks at 1558, 1405, and 1023 cm^{-1} also decreased. Similar results were found in biodegradable thermoplastic starch films with natural rosin (X. Zhang et al., 2022) and chitosan-resin nanofibers (Nirmala et al., 2013).

The films incorporated with ZnO nanoparticles exhibited alterations in their characteristic spectral peaks. A comparison between the spectra of films without and with the addition of ZnO nanoparticles reveals a shift towards both lower and higher wavenumber regions, particularly notable in the characteristic bands around 3260–3273 cm^{-1}. Mujeeb Rahman et al. (2018) and Z. Liu et al. (2016) similarly observed shifts in the position of spectral peaks in chitosan films upon the incorporation of ZnO nanoparticles. They attributed these shifts to a stronger interaction between the functional groups and the ZnO particles.

3.6. X-ray diffraction

X-ray diffraction provides information about the crystalline and amorphous phases present in polymers (Xu et al., 2019). The x-ray

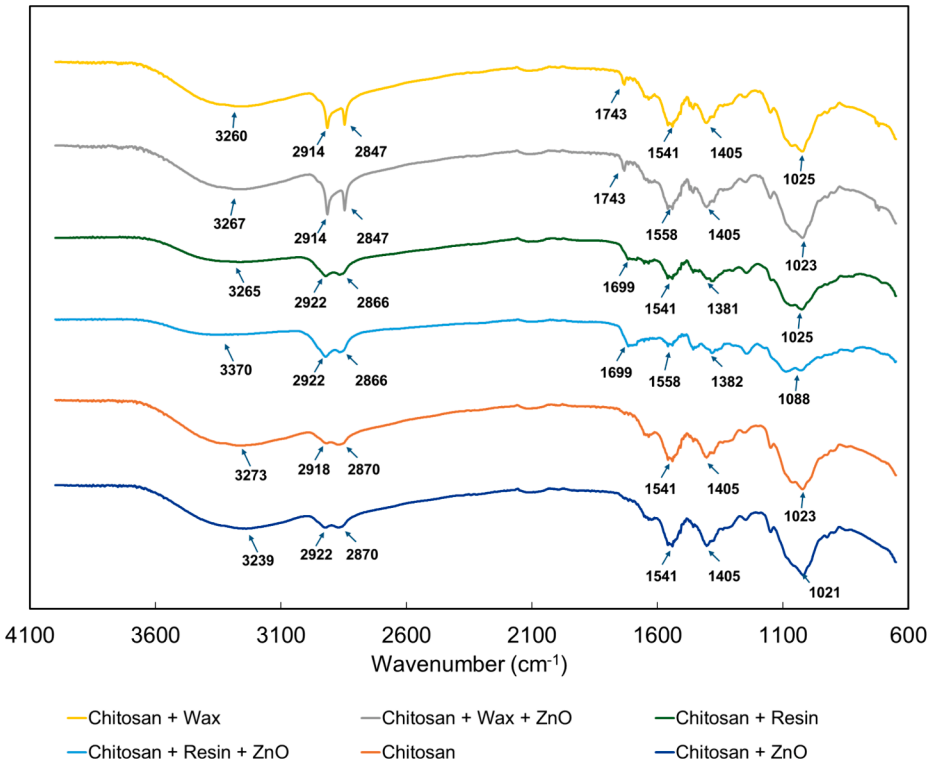

Fig. 4. FT-IR spectra of chitosan-based films.

diffractograms of different films are shown in Fig. 5.

The broad diffraction peak between 19 and 21° in the chitosan-only film defines its semicrystalline nature which points to the presence of a tight arrangement of polymer molecules attributed to strong intermolecular hydrogen bonds (Lin et al., 2023). Other authors described this same diffraction peak for chitosan films prepared with acetic acid as solvent (Qiao et al., 2021; Heping Wang et al., 2019; Ziani et al., 2008).

The addition of rosin resin to the chitosan-based films induced a leftward shift in the peak. The peak located at 18.15——19.31° corresponds to a basal interplanar spacing of 4.80——4.60 Å. It's noteworthy that this peak exhibits a broader and less intense profile when compared to the chitosan-only films. The amorphous nature of rosin resin, along with carboxylic acid groups in its composition, suggests that rosin seamlessly accommodated with the amorphous phase of chitosan within the composite structure (Cruces et al., 2021; Gaillard et al., 2011).

Carnauba wax films exhibited peaks of 2θ = 20.81 – 21.21° and 23.21—23.45°, corresponding to the basal interplanar spacing of 4.27——4.19 Å and 3.83——3.79 Å, respectively. According to Donhowe & Fennema (1993) and Paulo et al. (2019), these results indicate that wax films are partially crystalline and with characteristics of orthorhombic subcellular packing in lipids, which result in harder and less deformable films. Such effect was observed in the puncture force of the CW films. Furthermore, the peaks at 3.73 Å and 4.13 Å are known to represent short spacings, indicating the side-by-side orientation of the

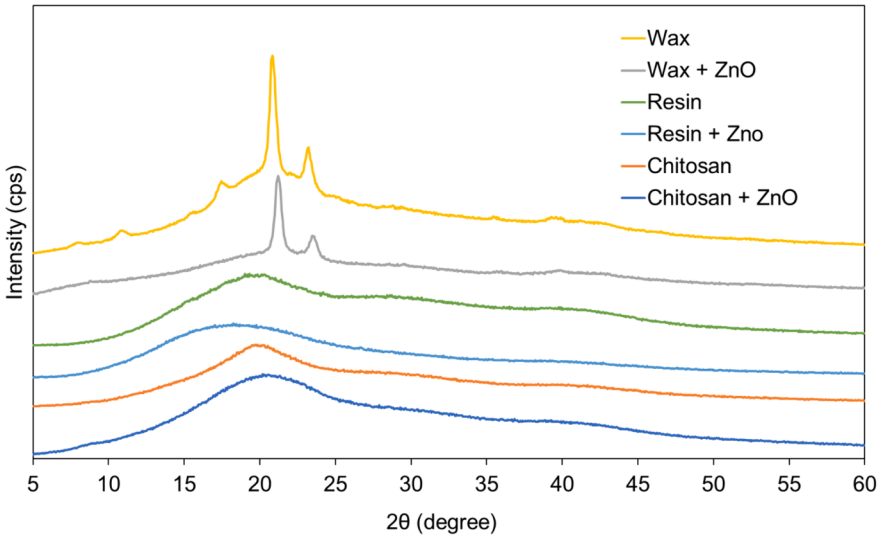

Fig. 5. XRD patterns of chitosan-based films.

hydrocarbon chains (Muscat et al., 2013).

The films incorporated with ZnO nanoparticles showed peaks at angles close to those of films without ZnO nanoparticles, with equal or close values of basal interplanar spacing (d), as it can be seen in Table 3. The unchanged or close values of the basal interplanar spacing suggest that a nanocomposite was formed. Furthermore, as can be seen in Fig. 5, all intensity peaks in the film incorporated with ZnO nanoparticles were reduced compared to films without ZnO nanoparticles. Thus, both the unchanged or close values of the basal interplanar spacing as well as the decrease in intensity and broadening of the peak suggest the formation of a nanocomposite (Sani et al., 2019).

3.7. Thermogravimetry analysis

The thermogravimetric analysis was performed to evaluate the effect of adding wax or resin as well as the incorporation of ZnO nanoparticles on the thermal stability of chitosan-based films. The weight losses of the different films are depicted in Fig. 6 and Table 4. Three primary stages of weight loss have been identified for chitosan-based films, and all of them were influenced by the presence of wax, resin and ZnO nanoparticles.

Between 25 and 220 °C the adsorbed water is lost, followed by the glycerol compounds, the residual acetic acid, and structurally bound water. Until 100 °C, the addition of ZnO or wax resulted in a greater weight loss, while the presence of resin was responsible for reducing the weight loss in around 60 % during this period. During this first step, however, the main changes on thermal degradation due to the different treatments was observed above 100 °C, when most of the organic compounds are consumed. Chitosan films presented 8.44 % of mass loss at this point, while all the different treatments resulted in smaller amounts of mass loss.

The second stage of thermal decomposition on chitosan films occurred from 228.67 to 414.33 °C. Higher losses were verified at this stage, which can be attributed to the dehydration of saccharide rings, depolymerization, and the decomposition of both acetylated and deacetylated units within the polymer (Singh & Dutta, 2011). The addition of carnauba wax and ZnO nanoparticles to the film composition led to the onset of degradation at early stages, approximately at 190 °C. This signifies a marginal decrease in the thermal resistance of the films. CW films presented another degradation step that reached maximum degradation rate at 430 °C, which is consistent with the presence of carnauba wax in biobased films (de Oliveira Filho et al., 2020). CWZn films showed a degradation with a maximum degradation at 414 °C, indicating not only that the presence of carnauba wax in the chitosan films can be observed as a singular event during degradation but also that it is affected by the presence of ZnO particles. The third main stage of degradation was observed between 400 and 500 °C can be attributed to thermal degradation of polysorbate 80 (Cárdenas & Miranda, 2004; W. Zhang et al., 2023). The reduction in weight loss persists slightly beyond 500 °C and is linked to the decomposition of C–C, C-O, and C-N single bonds in chitosan (Montaser et al., 2019).

3.8. DSC analysis

DSC is a method that provides information on the stability, degradation, melting (T_m) and glass transition temperature (T_g) of biopolymers used in food packaging subject to thermal changes (Gheribi et al., 2018). Therefore, DSC analysis was conducted to evaluate the thermal transition of chitosan-based films. The T_m and enthalpy associated with melting (ΔH) of the film samples are shown in Table 5 and DSC thermograms are shown in Fig. 7. The glass transition temperature could not be observed for chitosan-based films. According to Chiumarelli & Hubinger (2014), the T_g of polymeric films with plasticizer is difficult to determine by DSC analysis, since the variation in thermal capacity is very low in the glass transition.

Except for the resin films, two endothermic peaks were observed. The first peak ranging from 72.41 to 85.07 °C and the second peak between 213.95 and 235.76 °C. The first endothermic peak can be attributed to evaporation of water content and traces of acetic acid

Table 3
2θ and d values of chitosan-based films.

Treatment	2θ (°)	d (Å)
Chitosan	19.85	4.47
Chitosan + ZnO	20.19	4.40
Wax	20.82	4.27
	23.21	3.83
Wax + ZnO	21.21	4.19
	23.45	3.79
Resin	19.31	4.60
Resin + ZnO	18.15	4.89

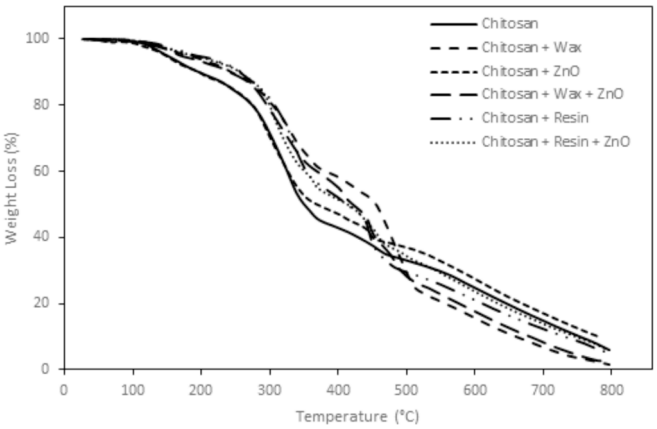

Fig. 6. Thermogravimetric analysis curves of chitosan-based films.

Table 4
Percentage weight loss obtained by thermogravimetric analysis of the chitosan-based films.

T	First stage	Second stage		Third stage		Total loss (%)
	Weight Loss (%)	Tonset (°C)	Weight Loss (%)	Tonset (°C)	Weight Loss (%)	
C	8,44	266,00	45,53	452,00	7,91	61,88
CZn	5,95	255,88	43,24	440,00	9,57	58,77
CW	2,90	286,57	38,15	453,96	33,70	74,75
CWZn	5,18	267,24	38,75	461,30	30,31	74,24
CR	4,39	252,65	41,72	403,68	23,45	69,56
CRZn	4,64	246,27	35,88	431,98	14,43	54,95

T: Treatment; C: Chitosan; CZn: Chitosan + ZnO; CW: Wax; CWZn: Wax + ZnO; CR: Resin; CRZn: Resin + ZnO.

Table 5
Melting temperature and enthalpy of chitosan-based films.

Treatment	1st Peak		2nd Peak	
	T_{m1} (°C)	ΔH_1 (J·g^{-1})	T_{m2} (°C)	ΔH_2 (J·g^{-1})
C	72.41^{c} ± 0.67	2.21^{b} ± 0.28	225.75^{b} ± 3.12	167.03^{b} ± 9.05
CZn	79.24^{b} ± 0.08	7.88^{b} ± 0.14	224.46^{b} ± 3.42	160.80^{b} ± 3.50
CW	85.07^{a} ± 0.83	48.65^{a} ± 8.07	234.76^{a} ± 0.32	94.18^{a} ± 1.43
CWZn	84.18^{a} ± 0.14	46.40^{a} ± 1.33	229.44^{ab} ± 1.13	91.44^{a} ± 2.98
CR	–	–	234.01^{a} ± 0.71	78.03^{a} ± .6.63
CRZn	–	–	232.95^{a} ± 2.22	89.25^{a} ± 7.75

C: Chitosan; CZn: Chitosan + ZnO; CW: Wax; CWZn: Wax + ZnO; CR: Resin; CRZn: Resin + ZnO. *The means followed by the same letter, in the columns, do not differ from each other, according to Tukey's test at 5 % probability.

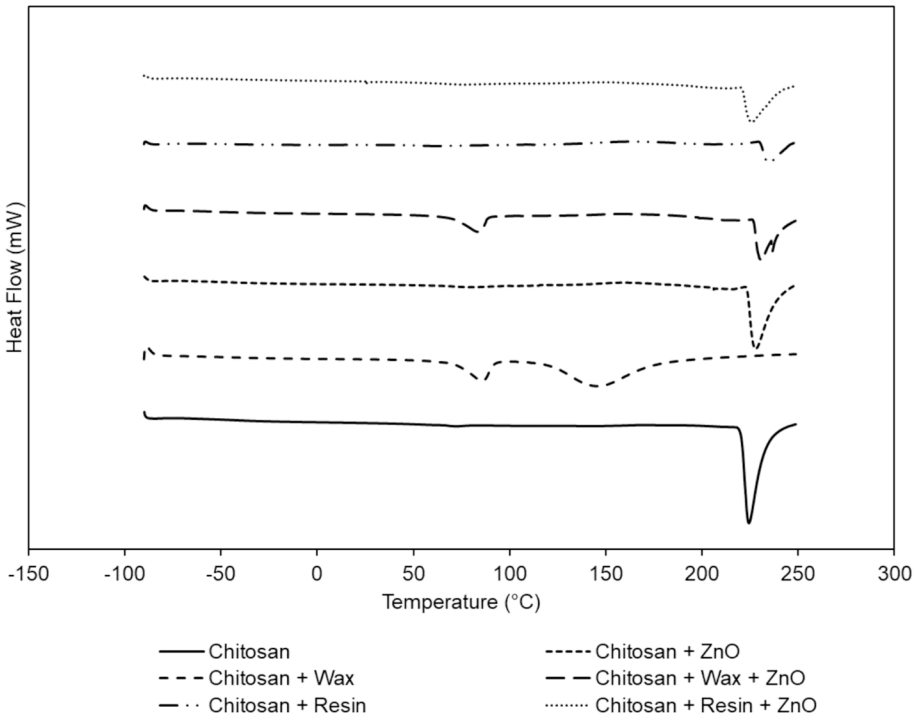

Fig. 7. DSC thermograms of chitosan-based films.

solvent. While the second and more prominent endothermic peak can be related to glycerol denaturation as well as depolymerization and decomposition of chitosan chains.

These results are in agreement with those found by de Oliveira et al. (2020) in chitosan films with lemongrass essential oil. Still, according to Zibaei et al. (2021), two phenomena can occur during the thermal degradation of most hydrocolloids: the chain stripping, which is caused by the removal of water molecules (dehydration), followed by the splitting and decomposition of the polymeric chain.

The first endothermic peak was less prominent on both pure chitosan and CZnO films, and the addition of ZnO did not alter the second peak. For carnauba wax films, the first endothermic peak was observed around 85 °C, which is related to the melting of wax crystals and is related to the increase in ΔH, as enthalpy of fusion reflects the crystallinity of the polymer (Kong & Hay, 2002). A second endothermic peak was found between 229 and 236 °C, which is related to the degradation of chitosan polymeric chains. As it can be seen in Table, the addition of carnauba wax resulted in a reduced ΔH during the second melting. Similar results were found in chitosan films with beeswax (Y. Liu et al., 2021) and polylactic acid films with carnauba wax (Wang et al., 2023).

Resin films, on the other hand, only presented one degradation peak, between the temperatures of 213 and 234 °C, which can be associated to the melting of the long chain polymers. The absence of a first endothermic peak that is associated with water loss is consistent with the reduced weight loss below 100 °C observed in the thermogravimetry analysis. Also, the only peak observed around 230 °C presented lower ΔH compared to pristine chitosan films, which is consistent with the findings of the XRD analysis of lower crystallinity of the CR and CRZn films.

3.9. Gas barrier properties

Films play an important role in the field of food packaging or coatings which is the ability to reduce water transfer between the packaged product and the external environment. Thus, the water loss of the product can be reduced, thus increasing the shelf life of these products (Hosseini et al., 2016; Yadav et al., 2021). The results of the water vapor, oxygen, and carbon dioxide permeability of chitosan-based films are shown in Table 6, which ranged from 0.32 to 0.52 $g{\cdot}mm{\cdot}h^{-1}{\cdot}m^{-2}{\cdot}kPa^{-1}$, 0 to 1.75 barrer, and 0.71 to 2.54 barrer, respectively.

CRZn, CR and CWZn films showed the lowest water vapor permeability, followed by wax film. Furthermore, the water vapor permeability reduced by 13,5% and 32,6% after incorporation of wax and resin in chitosan-based films, respectively. Regarding the films with ZnO nanoparticles, a reduction in water vapor permeability was observed after the incorporation of ZnO nanoparticles, except for the resin films.

Other studies also have evaluated water vapor permeability after the addition of hydrophobic compounds in polymeric film formulations. Hosseini et al. (2016) produced active films based on nanoparticles of gelatine and chitosan with the incorporation of different oregano essential oil concentrations. The authors observed that the maximum water vapor permeability of the films (34 %) was when 0.8 %(w/v) of essential oil was added to the film formulation. On the other hand, the water vapor permeability tended to increase with larger amounts of incorporated essential oil. Yadav et al. (2021) produced chitosan films containing ZnO nanoparticles loaded gallic-acid and observed that the increase of ZnO nanoparticles in the films led to a decrease in water vapor permeability values. According to the authors, this result was due

Table 6
Water vapor, oxygen, and carbon dioxide permeability of chitosan-based films.

T	Water vapor ($g{\cdot}mm{\cdot}h^{-1}{\cdot}m^{-2}{\cdot}kPa^{-1}$)	Oxygen (barrer)	Carbon dioxide (barrer)
C	$0.52^{c} \pm 0.03$	$1.75^{c} \pm 0.16$	$2.54^{d} \pm 0.08$
CZn	$0.46^{b} \pm 0.03$	$0.51^{b} \pm 0,04$	$2.48^{d} \pm 0.02$
CW	$0.45^{b} \pm 0.02$	nd	$1.81^{c} \pm 0.10$
CWZn	$0.37^{a} \pm 0.02$	nd	$0.64^{a} \pm 0.03$
CR	$0.35^{a} \pm 0.01$	$0,18^{a} \pm 0.02$	$0.91^{b} \pm 0.02$
CRZn	$0.32^{a} \pm 0.02$	nd	$0.71^{a} \pm 0.04$

*The means followed by the same letter, in the columns, do not differ from each other, according to Tukey's test at 5 % probability. T: Treatment; C: Chitosan; CZn: Chitosan + ZnO; CW: Wax; CWZn: Wax + ZnO; CR: Resin; CRZn: Resin + ZnO; 1 barrer $= \frac{1 \times 10^{-10} cm^3[STP] \bullet cm}{cm^2 \bullet s \bullet cmHg}$; nd: not detected.

to the ZnO nanoparticles occupying the voids in the structure of the macromolecular network, increasing the interaction between the chitosan molecules and the ZnO nanoparticles and compressing the interspace for the diffusion of water vapor.

The lipids are known to improve the water barrier properties of polymer-based films due to their hydrophobic character and decrease the water absorption capacity of the films (Sánchez-González et al., 2010). In addition, Hromiš et al. (2015) reported that water transfer in films is affected by different factors when hydrophobic components are added into film formulations. There is the effect of the hydrophobic nature of the polymeric matrix and the effect of the polymer-lipid interaction on the binding forces of the chains in the network. Water vapor permeability is limited when the increase in the hydrophobic nature of the matrix predominates over the effect of loss of matrix cohesion (Wang et al., 2022). If these two effects are balanced, no change in water vapor transfer will be observed.

The transfer of oxygen from the environment to food has an important effect on food quality and shelf life, since oxygen and carbon dioxide are essential for respiration in living tissue, such as fresh fruits and vegetables (Ayranci & Tunc, 2003). Regarding oxygen and carbon dioxide permeability, chitosan-based films showed low oxygen and carbon dioxide permeability. These results showed a similar trend to water vapor permeability values. That is, the addition of wax or resin decreased the permeability values for oxygen and carbon dioxide. This same behaviour was found after the incorporation of ZnO particles in the film formulations. In addition, wax films were less permeable to oxygen, while resin films were less permeable to carbon dioxide.

Similar results were found by Zhang et al. (2021) who evaluated the effect of addition of tannic acid to chitosan/gelatin composite films on the oxygen barrier properties e Yadav et al. (2021) studied the incorporation of zinc oxide nanoparticles in chitosan-based films. Both authors observed that the vapor oxygen permeability of the polymeric films decreased after the incorporation of tannic acid and ZnO nanoparticles, respectively. According Zhang et al. (2021) this result can be attributed to the fact that the tannic acid molecule distributed on the surface of the composite films occupied the perpendicularly diffusive pathway for oxygen. That is, the penetrating molecules travelled in a more tortuous diffusion path, which resulted in a decrease in oxygen permeability.

4. Conclusions

In this study, nanocomposite films were successfully developed using carnauba wax or rosin resin and ZnO nanoparticles to the chitosan matrix. The properties of chitosan-based films were influenced by the incorporation of resin or carnauba wax and ZnO nanoparticles. Wax or resin films and films with incorporated ZnO nanoparticles were less transparent than chitosan-only films, as well as presenting lower moisture content, water solubility, swelling. The SEM images revealed that the chitosan films exhibited a smoother and more uniform surface, whereas the carnauba wax films presented structural irregularities and roughness, attributed to their hydrophobic properties. However, the resin films exhibited surface heterogeneity, with rosin droplets dispersed within the chitosan matrix.

CZn and CRZn films showed higher tensile strength (36.74 ± 3.03 and 25.29 ± 1.92 MPa), higher Young's modulus (21.12 ± 2.05 and 20.74 ± 1.38) and lower elongation at break (3.39 ± 1.00 and 4.34 ± 0.71 %). Furthermore, the moisture content, water solubility, and swelling of the CRZn films were 21.47 ± 0.60, 16.47 ± 0.18, and 68.53 ± 0.94, respectively.

Overall, films produced resin with ZnO nanoparticles (CRZn) showed improvements in mechanical and optical properties as well as gas and light barrier properties, mainly due to their low water solubility, higher elongation at break, good UV protection and low permeability to water vapor and oxygen. Thus, the use of this formulation in future applications, such as packaging materials and coatings is a promising alternative to increase the shelf life of food products, mainly for exporting fresh fruits.

Funding

This work was supported by CAPES – Coordenação de Aperfeiçoamento de Pessoal de Nível Superior (grant #88887.646273/2021–00) and FAPERJ – Fundação de Amparo à Pesquisa do Estado do Rio de Janeiro, Brazil (grant #E-26/204.362/2021 and E-26/203.198/2019).

CRediT authorship contribution statement

Luiz Carlos Corrêa-Filho: Writing – review & editing, Writing – original draft, Visualization, Methodology, Formal analysis, Conceptualization. **Jailton Ribeiro dos Santos Junior:** Investigation, Formal analysis, Data curation, Conceptualization. **Andresa Viana Ramos:** Writing – review & editing, Investigation. **Ana Paula Martinazzo:** Resources, Investigation. **Alberto Claudio Habert:** Resources, Investigation. **Carlos Wanderlei Piler de Carvalho:** Writing – review & editing, Methodology. **Antônio Gomes Soares:** Writing – review & editing, Methodology, Investigation, Formal analysis, Data curation, Conceptualization. **Renata Valeriano Tonon:** Writing – review & editing, Visualization, Methodology, Conceptualization. **Lourdes Maria Corrêa Cabral:** Conceptualization, Formal analysis, Funding acquisition, Methodology, Project administration, Resources, Supervision, Visualization, Writing – review & editing.

Declaration of competing interest

The authors declare that they have no known competing financial interests or personal relationships that could have appeared to influence the work reported in this paper.

Data availability

Data will be made available on request.

Acknowledgements

The authors are grateful to Centro Nacional de Biologia Estrutural e Bioimagem (CENABIO) for the access to the Quattro SEM.

References

Akhtar, M., Butt, M. S., Maan, A. A., & Asghar, M. (2022). Development and characterization of emulsion-based films incorporated with chitosan and sodium caseinate. *Journal of Food Measurement and Characterization, 16*(4), 3278–3288. https://doi.org/10.1007/S11694-022-01422-1/TABLES/3

Al-Naamani, L., Dobretsov, S., & Dutta, J. (2016). Chitosan-zinc oxide nanoparticle composite coating for active food packaging applications. *Innovative Food Science & Emerging Technologies, 38*, 231–237. https://doi.org/10.1016/J.IFSET.2016.10.010

Asioli, D., Aschemann-Witzel, J., Caputo, V., Vecchio, R., Annunziata, A., Næs, T., & Varela, P. (2017). Making sense of the "clean label" trends: A review of consumer food choice behavior and discussion of industry implications. *Food Research International, 99*, 58–71. https://doi.org/10.1016/J.FOODRES.2017.07.022

ASTM. (1993). *Annual Book of American Standard Testing Methods*.

Ayranci, E., & Tunc, S. (2003). A method for the measurement of the oxygen permeability and the development of edible films to reduce the rate of oxidative reactions in fresh foods. *Food Chemistry, 80*(3), 423–431. https://doi.org/10.1016/S0308-8146(02)00485-5

Butt, M. S., Akhtar, M., Maan, A. A., & Asghar, M. (2023). Fabrication and characterization of carnauba wax-based films incorporated with sodium alginate/whey protein. *Journal of Food Measurement and Characterization, 17*(1), 694–705. https://doi.org/10.1007/S11694-022-01636-3/TABLES/3

Cárdenas, G., & Miranda, S. P. (2004). FTIR AND TGA STUDIES OF CHITOSAN COMPOSITE FILMS. *Journal of the Chilean Chemical Society, 49*(4), 291–295. https://doi.org/10.4067/S0717-97072004000400005

Cazón, P., Vázquez, M., & Velazquez, G. (2019). Composite Films with UV-Barrier Properties Based on Bacterial Cellulose Combined with Chitosan and Poly(vinyl alcohol): Study of Puncture and Water Interaction Properties. *Biomacromolecules, 20*(5), 2084–2095. https://doi.org/10.1021/ACS.BIOMAC.9B00317/ASSET/IMAGES/LARGE/BM-2019-00317W_0007.JPEG

Chen, H., Hu, X., Chen, E., Wu, S., McClements, D. J., Liu, S., Li, B., & Li, Y. (2016). Preparation, characterization, and properties of chitosan films with cinnamaldehyde nanoemulsions. *Food Hydrocolloids, 61*, 662–671. https://doi.org/10.1016/J.FOODHYD.2016.06.034

Chiumarelli, M., & Hubinger, M. D. (2014). Evaluation of edible films and coatings formulated with cassava starch, glycerol, carnauba wax and stearic acid. *Food Hydrocolloids, 38*, 20–27. https://doi.org/10.1016/J.FOODHYD.2013.11.013

Teixeira, J.A., Freitas-Silva, O., & Cabral, L.M.C. (2020). Cellulose nanocrystals from grape pomace and their use for the development of starch-based nanocomposite films. *International Journal of Biological Macromolecules*, *159*, 1048–1061. doi: 10.1016/J.IJBIOMAC.2020.05.046.

Cortés-Rodríguez, M., Villegas-Yépez, C., Gil González, J. H., Rodríguez, P. E., & Ortega-Toro, R. (2020). Development and evaluation of edible films based on cassava starch, whey protein, and bees wax. *Heliyon, 6*(9), e04884.

Cruces, F., García, M. G., & Ochoa, N. A. (2021). Reduction of Water Vapor Permeability in Food Multilayer Biopackaging by Epitaxial Crystallization of Beeswax. *Food and Bioprocess Technology, 14*(7), 1244–1255. https://doi.org/10.1007/S11947-021-02628-9/FIGURES/5

de Moraes Crizel, T., de Oliveira Rios, A., D. Alves, V., Bandarra, N., Moldão-Martins, M., & Hickmann Flôres, S. (2018). Active food packaging prepared with chitosan and olive pomace. *Food Hydrocolloids*, *74*, 139–150. doi: 10.1016/J.FOODHYD.2017.08.007.

de Oliveira, L. I. G., de Oliveira, K.Á. R., de Medeiros, E. S., Batista, A. U. D., Madruga, M. S., dos Santos Lima, M., de Souza, E. L., & Magnani, M. (2020). Characterization and efficacy of a composite coating containing chitosan and lemongrass essential oil on postharvest quality of guava. *Innovative Food Science & Emerging Technologies, 66*, Article 102506. https://doi.org/10.1016/J.IFSET.2020.102506

Díaz-montes, E., & Castro-muñoz, R. (2021). Trends in Chitosan as a Primary Biopolymer for Functional Films and Coatings Manufacture for Food and Natural Products. *Polymers 2021, Vol. 13, Page 767*, *13*(5), 767. doi: 10.3390/POLYM13050767.

Donhowe, G., & Fennema, O. (1993). Water vapor and oxygen permeability of wax films. *Journal of the American Oil Chemists' Society, 70*(9), 867–873. https://doi.org/10.1007/BF02545345

Dos Santos, F. K. G., De Oliveira Silva, K. N., Xavier, T. D. N., De Lima Leite, R. H., & Aroucha, E. M. M. (2017). Effect of the Addition of Carnauba Wax on Physicochemical Properties of Chitosan Films. *Materials Research, 20*, 479–484. https://doi.org/10.1590/1980-5373-MR-2016-1010

Espitia, P.J.P., Soares, N. de F.F., Coimbra, J.S. dos R., de Andrade, N.J., Cruz, R. S., & Medeiros, E.A.A. (2012). Zinc Oxide Nanoparticles: Synthesis, Antimicrobial Activity and Food Packaging Applications. *Food and Bioprocess Technology 2012 5:5*, *5*(5), 1447–1464. doi: 10.1007/S11947-012-0797-6.

Gaillard, Y., Mija, A., Burr, A., Darque-Ceretti, E., Felder, E., & Sbirrazzuoli, N. (2011). Green material composites from renewable resources: Polymorphic transitions and phase diagram of beeswax/rosin resin. *Thermochimica Acta, 521*(1–2), 90–97. https://doi.org/10.1016/J.TCA.2011.04.010

García Jiménez, C. D., Habert, A. C., & Borges, C. P. (2021). Polyurethane/polyethersulfone dual-layer anisotropic membranes for CO2 removal from flue gas. *Journal of Applied Polymer Science, 138*(21), 50476. https://doi.org/10.1002/APP.50476

Gheribi, R., Puchot, L., Verge, P., Jaoued-Grayaa, N., Mezni, M., Habibi, Y., & Khwaldia, K. (2018). Development of plasticized edible films from Opuntia ficus-indica mucilage: A comparative study of various polyol plasticizers. *Carbohydrate Polymers, 190*, 204–211. https://doi.org/10.1016/J.CARBPOL.2018.02.085

Ghiasi, F., Golmakani, M. T., Eskandari, M. H., & Hosseini, S. M. H. (2020). A new approach in the hydrophobic modification of polysaccharide-based edible films using structured oil nanoparticles. *Industrial Crops and Products, 154*, Article 112679. https://doi.org/10.1016/J.INDCROP.2020.112679

Gomes, Á. V. R., Gonçalves, F. C. P., da Silva, M. Q., de Lima Leite, R. H., dos Santos, F. K. G., & Aroucha, E. M. M. (2019). Effect of Carnauba Wax and Coconut Fiber Contents on Tensile Properties of Corn Starch-Based Biocomposites. *Materials Research, 22*, e20190053.

Gutiérrez-Pacheco, M.M., Ortega-Ramírez, L.A., Silva-Espinoza, B.A., Cruz-Valenzuela, M.R., González-Aguilar, G.A., Lizardi-Mendoza, J., Miranda, R., & Ayala-Zavala, J.F. (2020). Individual and Combined Coatings of Chitosan and Carnauba Wax with Oregano Essential Oil to Avoid Water Loss and Microbial Decay of Fresh Cucumber. *Coatings 2020, Vol. 10, Page 614*, *10*(7), 614. doi: 10.3390/COATINGS10070614.

Hosseini, S. F., Rezaei, M., Zandi, M., & Farahmandghavi, F. (2016). Development of bioactive fish gelatin/chitosan nanoparticles composite films with antimicrobial properties. *Food Chemistry, 194*, 1266–1274. https://doi.org/10.1016/J.FOODCHEM.2015.09.004

Hromiš, N. M., Lazić, V. L., Markov, S. L., Vaštag, Ž. G., Popović, S. Z., Šuput, D. Z., Džinić, N. R., Velićanski, A. S., & Popović, L. M. (2015). Optimization of chitosan biofilm properties by addition of caraway essential oil and beeswax. *Journal of Food Engineering, 158*, 86–93. https://doi.org/10.1016/J.JFOODENG.2015.01.001

Kamarudin, S.H., Rayung, M., Abu, F., Ahmad, S., Fadil, F., Karim, A.A., Norizan, M.N., Sarifuddin, N., Desa, M.S.Z.M., Basri, M.S.M., Samsudin, H., & Abdullah, L.C. (2022). A Review on Antimicrobial Packaging from Biodegradable Polymer Composites. *Polymers 2022, Vol. 14, Page 174*, *14*(1), 174. doi: 10.3390/POLYM14010174.

Khalid, M. Y., & Arif, Z. U. (2022). Novel biopolymer-based sustainable composites for food packaging applications: A narrative review. *Food Packaging and Shelf Life, 33*, Article 100892. https://doi.org/10.1016/J.FPSL.2022.100892

Kong, Y., & Hay, J. N. (2002). The measurement of the crystallinity of polymers by DSC. *Polymer, 43*(14), 3873–3878. https://doi.org/10.1016/S0032-3861(02)00235-5

Lin, Y., Qiao, C., Zhao, Z., Xia, Y., Zhao, G., & Xue, Z. (2023). Fabrication and Characterization of Carrageenan/ZnO/Chitosan Composite Films. *Langmuir*. https://doi.org/10.1021/ACS.LANGMUIR.3C00791

Liu, Y., Ma, Y., Feng, T., Luo, J., Sameen, D. E., Hossen, M. A., Dai, J., Li, S., & Qin, W. (2021). Development and characterization of aldehyde-sensitive cellulose/chitosan/beeswax colorimetric papers for monitoring kiwifruit maturity. *International Journal of Biological Macromolecules, 187*, 566–574. https://doi.org/10.1016/J.IJBIOMAC.2021.07.132

Liu, Z., Lv, M., Li, F., & Zeng, M. (2016). Development, Characterization, and Antimicrobial Activity of Gelatin/Chitosan/ZnO Nanoparticle Composite Films. *Journal of Aquatic Food Product Technology, 25*(7), 1056–1063. https://doi.org/10.1080/10498850.2014.923081

Martins, J. T., Cerqueira, M. A., & Vicente, A. A. (2012). Influence of α-tocopherol on physicochemical properties of chitosan-based films. *Food Hydrocolloids, 27*(1), 220–227. https://doi.org/10.1016/J.FOODHYD.2011.06.011

Mei, J., Yuan, Y., Wu, Y., & Li, Y. (2013). Characterization of edible starch–chitosan film and its application in the storage of Mongolian cheese. *International Journal of Biological Macromolecules, 57*, 17–21. https://doi.org/10.1016/J.IJBIOMAC.2013.03.003

Meindrawan, B., Suyatma, N. E., Wardana, A. A., & Pamela, V. Y. (2018). Nanocomposite coating based on carrageenan and ZnO nanoparticles to maintain the storage quality of mango. *Food Packaging and Shelf Life, 18*, 140–146. https://doi.org/10.1016/J.FPSL.2018.10.006

Mesías, F. J., Martín, A., & Hernández, A. (2021). Consumers' growing appetite for natural foods: Perceptions towards the use of natural preservatives in fresh fruit. *Food Research International, 150*, Article 110749. https://doi.org/10.1016/J.FOODRES.2021.110749

Moeini, A., Germann, N., Malinconico, M., & Santagata, G. (2021). Formulation of secondary compounds as additives of biopolymer-based food packaging: A review. *Trends in Food Science & Technology, 114*, 342–354. https://doi.org/10.1016/J.TIFS.2021.05.040

Mohammadi, H., Kamkar, A., Misaghi, A., Zunabovic-Pichler, M., & Fatehi, S. (2019). Nanocomposite films with CMC, okra mucilage, and ZnO nanoparticles: Extending the shelf-life of chicken breast meat. *Food Packaging and Shelf Life, 21*, Article 100330. https://doi.org/10.1016/J.FPSL.2019.100330

Montaser, A. S., Wassel, A. R., & Al-Shaye'a, O. N. (2019). Synthesis, characterization and antimicrobial activity of Schiff bases from chitosan and salicylaldehyde/TiO2 nanocomposite membrane. *International Journal of Biological Macromolecules, 124*, 802–809. https://doi.org/10.1016/J.IJBIOMAC.2018.11.229

Mujeeb Rahman, P., Abdul Mujeeb, V. M., Muraleedharan, K., & Thomas, S. K. (2018). Chitosan/nano ZnO composite films: Enhanced mechanical, antimicrobial and dielectric properties. *Arabian Journal of Chemistry, 11*(1), 120–127. https://doi.org/10.1016/J.ARABJC.2016.09.008

Muscat, D., Adhikari, R., McKnight, S., Guo, Q., & Adhikari, B. (2013). The physicochemical characteristics and hydrophobicity of high amylose starch–glycerol films in the presence of three natural waxes. *Journal of Food Engineering, 119*(2), 205–219. https://doi.org/10.1016/J.JFOODENG.2013.05.033

Ngo, T. M. P., Dang, T. M. Q., Tran, T. X., & Rachtanapun, P. (2018). Effects of Zinc Oxide Nanoparticles on the Properties of Pectin/Alginate Edible Films. *International Journal of Polymer Science, 2018*. https://doi.org/10.1155/2018/5645797

Nirmala, R., Woo-il, B., Navamathavan, R., Kalpana, D., Lee, Y. S., & Kim, H. Y. (2013). Influence of antimicrobial additives on the formation of rosin nanofibers via electrospinning. *Colloids and Surfaces. B, Biointerfaces, 104*, 262–267. https://doi.org/10.1016/J.COLSURFB.2012.12.014

Oliva-Moreno, E. E., & Encinas, A. (2021). Addition of Pine Rosin to Pectin bioplastic films for improved water resistance. *Materials Letters, 290*, Article 129488. https://doi.org/10.1016/J.MATLET.2021.129488

Oliveira Filho, J.G. de, Bezerra, C.C. de O.N., Albiero, B.R., Oldoni, F.C.A., Miranda, M., Egea, M.B., Azeredo, H.M.C. de, & Ferreira, M.D. (2020). New approach in the development of edible films: The use of carnauba wax micro- or nanoemulsions in arrowroot starch-based films. *Food Packaging and Shelf Life*, *26*, 100589. doi: 10.1016/J.FPSL.2020.100589.

Paulo, B. B., Schmiele, M., Maximo, G. J., & Prata, A. S. (2019). Carnauba Wax Particles: Investigation of Dripping and Cold-Extrusion Processes. *Journal of the American Oil Chemists' Society, 96*(7), 847–859. https://doi.org/10.1002/AOCS.12224

Pelissari, F.M., Andrade-Mahecha, M.M., Sobral, P.J. do A., & Menegalli, F.C. (2013). Comparative study on the properties of flour and starch films of plantain bananas (Musa paradisiaca). *Food Hydrocolloids*, *30*(2), 681–690. doi: 10.1016/J.FOODHYD.2012.08.007.

Piñeros-Hernandez, D., Medina-Jaramillo, C., López-Córdoba, A., & Goyanes, S. (2017). Edible cassava starch films carrying rosemary antioxidant extracts for potential use as active food packaging. *Food Hydrocolloids, 63*, 488–495. https://doi.org/10.1016/J.FOODHYD.2016.09.034

Porto, R. C. T., Uchôa, P. Z., Peschel, L. T., Justi, B., Koslowski, L. A. D., & Nogueira, A. L. (2018). Nanopartículas de óxido de zinco sintetizadas pelo método poliol: caracterização e avaliação da atividade antibacteriana. *Matéria (Rio de Janeiro), 22*. https://doi.org/10.1590/S1517-707620170005.0248

Priyadarshi, R., & Rhim, J. W. (2020). Chitosan-based biodegradable functional films for food packaging applications. *Innovative Food Science & Emerging Technologies, 62*, Article 102346. https://doi.org/10.1016/J.IFSET.2020.102346

Qiao, C., Ma, X., Wang, X., & Liu, L. (2021). Structure and properties of chitosan films: Effect of the type of solvent acid. *LWT, 135*, Article 109984. https://doi.org/10.1016/J.LWT.2020.109984

Reza, M. S., Quadir, M. A., & Haider, S. S. (2003). Comparative evaluation of plastic, hydrophobic and hydrophilic polymers as matrices for controlled-release drug delivery. *J Pharm Pharm Sci, 6*(2), 282–291.

da Rocha, B. A., Francisco, C. R. L., de Almeida, M., Ames, F. Q., Bona, E., Leimann, F. V., Gonçalves, O. H., & Bersani-Amado, C. A. (2020). Antiinflammatory activity of carnauba wax microparticles containing curcumin. *Journal of Drug Delivery Science and Technology, 59*, Article 101918. https://doi.org/10.1016/J.JDDST.2020.101918

Rocha, G. O., Farias, M. G., De Carvalho, C. W. P., Ascheri, J. L. R., & Galdeano, M. C. (2014). Filmes compostos biodegradáveis a base de amido de mandioca e proteína de soja. *Polímeros, 24*(5), 587–595. https://doi.org/10.1590/0104-1428.1355

Sahraee, S., Ghanbarzadeh, B., Milani, J. M., & Hamishehkar, H. (2017). Development of Gelatin Bionanocomposite Films Containing Chitin and ZnO Nanoparticles. *Food and Bioprocess Technology, 10*(8), 1441–1453. https://doi.org/10.1007/S11947-017-1907-2/FIGURES/5

Sánchez-González, L., Cháfer, M., Chiralt, A., & González-Martínez, C. (2010). Physical properties of edible chitosan films containing bergamot essential oil and their inhibitory action on Penicillium italicum. *Carbohydrate Polymers, 82*(2), 277–283. https://doi.org/10.1016/J.CARBPOL.2010.04.047

Sani, I. K., Pirsa, S., & Tağı, Ş. (2019). Preparation of chitosan/zinc oxide/Melissa officinalis essential oil nano-composite film and evaluation of physical, mechanical and antimicrobial properties by response surface method. *Polymer Testing, 79*, Article 106004. https://doi.org/10.1016/J.POLYMERTESTING.2019.106004

Santacruz, S., Rivadeneira, C., & Castro, M. (2015). Edible films based on starch and chitosan. Effect of starch source and concentration, plasticizer, surfactant's hydrophobic tail and mechanical treatment. *Food Hydrocolloids, 49*, 89–94. https://doi.org/10.1016/J.FOODHYD.2015.03.019

Santos, T. M., Pinto, A. M. B., de Oliveira, A. V., Ribeiro, H. L., Caceres, C. A., Ito, E. N., & Azeredo, H. M. C. (2014). Physical properties of cassava starch–carnauba wax emulsion films as affected by component proportions. *International Journal of Food Science & Technology, 49*(9), 2045–2051. https://doi.org/10.1111/IJFS.12499

Shankar, S., & Rhim, J. W. (2016). Preparation of nanocellulose from micro-crystalline cellulose: The effect on the performance and properties of agar-based composite films. *Carbohydrate Polymers, 135*, 18–26. https://doi.org/10.1016/J.CARBPOL.2015.08.082

Shankar, S., Wang, L. F., & Rhim, J. W. (2018). Incorporation of zinc oxide nanoparticles improved the mechanical, water vapor barrier, UV-light barrier, and antibacterial properties of PLA-based nanocomposite films. *Materials Science and Engineering: C, 93*, 289–298. https://doi.org/10.1016/J.MSEC.2018.08.002

Singh, J., & Dutta, P. K. (2011). Antibacterial and Physiochemical Behavior of Prepared Chitosan/pyridine-3,5-di-carboxylic Acid Complex for Biomedical Applications. *Journal of Macromolecular Science, Part A, 48*(3), 246–253. https://doi.org/10.1080/10601325.2011.544959

Siripatrawan, U., & Harte, B. R. (2010). Physical properties and antioxidant activity of an active film from chitosan incorporated with green tea extract. *Food Hydrocolloids, 24*(8), 770–775. https://doi.org/10.1016/J.FOODHYD.2010.04.003

Soazo, M., Pérez, L. M., Rubiolo, A. C., & Verdini, R. A. (2013). Effect of freezing on physical properties of whey protein emulsion films. *Food Hydrocolloids, 31*(2), 256–263. https://doi.org/10.1016/J.FOODHYD.2012.10.022

Su, N., Fang, C., Zhou, H., Tang, T., Zhang, S., Wang, X., & Fei, B. (2021). Effect of Rosin Modification on the Visual Characteristics of Round Bamboo Culm. *Polymers 2021, Vol. 13, Page 3500*, *13*(20), 3500. doi: 10.3390/POLYM13203500.

Susmita Devi, L., Kalita, S., Mukherjee, A., & Kumar, S. (2022). Carnauba wax-based composite films and coatings: Recent advancement in prolonging postharvest shelf-life of fruits and vegetables. *Trends in Food Science & Technology, 129*, 296–305. https://doi.org/10.1016/J.TIFS.2022.09.019

Terzioğlu, P., Güney, F., Parın, F. N., Şen, İ., & Tuna, S. (2021). Biowaste orange peel incorporated chitosan/polyvinyl alcohol composite films for food packaging applications. *Food Packaging and Shelf Life, 30*, Article 100742. https://doi.org/10.1016/J.FPSL.2021.100742

Vieira, T.M., Moldão-Martins, M., & Alves, V.D. (2021). Design of Chitosan and Alginate Emulsion-Based Formulations for the Production of Monolayer Crosslinked Edible Films and Coatings. *Foods 2021, Vol. 10, Page 1654*, *10*(7), 1654. doi: 10.3390/FOODS10071654.

Wang, H., Gong, X., Miao, Y., Guo, X., Liu, C., Fan, Y. Y., Zhang, J., Niu, B., & Li, W. (2019). Preparation and characterization of multilayer films composed of chitosan, sodium alginate and carboxymethyl chitosan-ZnO nanoparticles. *Food Chemistry, 283*, 397–403. https://doi.org/10.1016/J.FOODCHEM.2019.01.022

Wang, H., Ding, F., Ma, L., & Zhang, Y. (2021). Edible films from chitosan-gelatin: Physical properties and food packaging application. *Food Bioscience, 40*, Article 100871. https://doi.org/10.1016/J.FBIO.2020.100871

Wang, L., Xu, J., Zhang, M., Zheng, H., & Li, L. (2022). Preservation of soy protein-based meat analogues by using PLA/PBAT antimicrobial packaging film. *Food Chemistry, 380*, Article 132022. https://doi.org/10.1016/J.FOODCHEM.2021.132022

Wang, X., Chen, K., Liu, Y., He, R., & Wang, Q. (2023). Preparation and application of biodegradable and superhydrophobic polylactic acid/carnauba wax coating. *Progress in Organic Coatings, 177*, Article 107434. https://doi.org/10.1016/J.PORGCOAT.2023.107434

Wardana, Suyatma, N.E., Muchtadi, T.R., & Yuliani. (2018). Influence of ZnO nanoparticles and stearic acid on physical, mechanical and structural properties of cassava starch-based bionanocomposite edible films. *International Food Research Journal*, *25*(5), 1837–1844.

Wu, C., Sun, J., Zheng, P., Kang, X., Chen, M., Li, Y., Ge, Y., Hu, Y., & Pang, J. (2019). Preparation of an intelligent film based on chitosan/oxidized chitin nanocrystals incorporating black rice bran anthocyanins for seafood spoilage monitoring. *Carbohydrate Polymers, 222*, Article 115006. https://doi.org/10.1016/J.CARBPOL.2019.115006

Xavier, T.D.N., de Oliveira, V.R.L., Leite, R.H. de L., Aroucha, E.M.M., & Dos Santos, F.K. G. (2020). Filmes biopoliméricos baseados em fécula, quitosana e cera de carnaúba e suas propriedades. *Matéria (Rio de Janeiro)*, *25*(4), e-12866. doi: 10.1590/S1517-707620200004.1166.

Xu, T., Gao, C. C., Feng, X., Yang, Y., Shen, X., & Tang, X. (2019). Structure, physical and antioxidant properties of chitosan-gum arabic edible films incorporated with cinnamon essential oil. *International Journal of Biological Macromolecules, 134*, 230–236. https://doi.org/10.1016/J.IJBIOMAC.2019.04.189

Yadav, S., Mehrotra, G. K., & Dutta, P. K. (2021). Chitosan based ZnO nanoparticles loaded gallic-acid films for active food packaging. *Food Chemistry, 334*, Article 127605. https://doi.org/10.1016/J.FOODCHEM.2020.127605

Zhang, C., Yang, Z., Shi, J., Zou, X., Zhai, X., Huang, X., Li, Z., Holmes, M., Daglia, M., & Xiao, J. (2021). Physical properties and bioactivities of chitosan/gelatin-based films loaded with tannic acid and its application on the preservation of fresh-cut apples. *LWT, 144*, Article 111223. https://doi.org/10.1016/J.LWT.2021.111223

Zhang, L., Liu, Z., Wang, X., Dong, S., Sun, Y., & Zhao, Z. (2019). The properties of chitosan/zein blend film and effect of film on quality of mushroom (Agaricus bisporus). *Postharvest Biology and Technology, 155*, 47–56. https://doi.org/10.1016/J.POSTHARVBIO.2019.05.013

Zhang, W., Zhou, W., Zhang, Z., Zhang, D., Guo, Z., Ren, P., & Liu, F. (2023). Effect of Nano-Silica and Sorbitol on the Properties of Chitosan-Based Composite Films. *Polymers 2023, Vol. 15, Page 4015*, *15*(19), 4015. doi: 10.3390/POLYM15194015.

Zhang, X., Ma, H., Qin, W., Guo, B., & Li, P. (2022). Antimicrobial and improved performance of biodegradable thermoplastic starch by using natural rosin to replace part of glycerol. *Industrial Crops and Products, 178*, Article 114613. https://doi.org/10.1016/J.INDCROP.2022.114613

Zhang, Y., Simpson, B. K., & Dumont, M. J. (2018). Effect of beeswax and carnauba wax addition on properties of gelatin films: A comparative study. *Food Bioscience, 26*, 88–95. https://doi.org/10.1016/J.FBIO.2018.09.011

Ziani, K., Oses, J., Coma, V., & Maté, J. I. (2008). Effect of the presence of glycerol and Tween 20 on the chemical and physical properties of films based on chitosan with different degree of deacetylation. *LWT - Food Science and Technology, 41*(10), 2159–2165. https://doi.org/10.1016/J.LWT.2007.11.023

Zibaei, R., Hasanvand, S., Hashami, Z., Roshandel, Z., Rouhi, M., Guimarães, J. de T., Mortazavian, A.M., Sarlak, Z., & Mohammadi, R. (2021). Applications of emerging botanical hydrocolloids for edible films: A review. *Carbohydrate Polymers*, *256*. doi: 10.1016/J.CARBPOL.2020.117554.